

The impact of fluctuations in intensity patterns on the number of monitor units and the quality and accuracy of intensity modulated radiotherapy

Radhe Mohan, Mark Arnfield, Shidong Tong, Qiuwen Wu, and Jeffrey Siebers

Citation: *Medical Physics* **27**, 1226 (2000); doi: 10.1118/1.599000

View online: <http://dx.doi.org/10.1118/1.599000>

View Table of Contents: <http://scitation.aip.org/content/aapm/journal/medphys/27/6?ver=pdfcov>

Published by the [American Association of Physicists in Medicine](#)

Articles you may be interested in

Intensity modulated proton therapy treatment planning using single-field optimization: The impact of monitor unit constraints on plan quality

Med. Phys. **37**, 1210 (2010); 10.1118/1.3314073

Effect of respiratory motion on the delivery of breast radiotherapy using SMLC intensity modulation

Med. Phys. **34**, 347 (2007); 10.1118/1.2405323

A new method of incorporating systematic uncertainties in intensity-modulated radiotherapy optimization

Med. Phys. **32**, 2567 (2005); 10.1118/1.1954161


Monte Carlo evaluation of 6 MV intensity modulated radiotherapy plans for head and neck and lung treatments

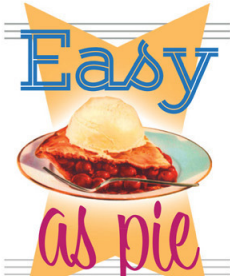
Med. Phys. **29**, 2705 (2002); 10.1118/1.1517291

Independent monitor unit calculation for intensity modulated radiotherapy using the MIMiC multileaf collimator

Med. Phys. **29**, 2041 (2002); 10.1118/1.1500397

Radhe Mohan, Mark Arnfield, Shidong Tong, Qiuwen Wu, and Jeffrey Siebers

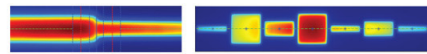




Easy
as pie

RITG148⁺


Custom Designed
TG-148 Tests
For Tomotherapy QA



RIT is your only source for the tests specified for helical tomotherapy in the TG-148 report. These automated QA tests include:

• Automated QA testing	• MLC alignment test
• Y-jaw divergence/beam centering	• Couch translation/gantry rotation
• Y-jaw/gantry rotation plane alignment	• Laser localization
• Gantry angle consistency	• Image quality tests (Cheese Phantom)
• Treatment field centering	• Built in trending and reporting with RITrend

These tests are included in both our RITComplete, and RITG148+ products.



Call 719.590.1077,
option 4, or email
mac@radimage.com
today to set up your
personal demo.

The impact of fluctuations in intensity patterns on the number of monitor units and the quality and accuracy of intensity modulated radiotherapy

Radhe Mohan,^{a)} Mark Arnfield, Shidong Tong, Qiuwen Wu, and Jeffrey Siebers
*Department of Radiation Oncology, Medical College of Virginia, Virginia Commonwealth University,
Richmond, Virginia 23298 and McGuire VA Hospital, Richmond, Virginia 23298*

(Received 22 September 1999; accepted for publication 22 March 2000)

The purpose of this work is to examine the potential impact of the frequency and amplitude of fluctuations (“complexity”) in intensity distributions on intensity-modulated radiotherapy (IMRT) dose distributions. The intensity-modulated beams are efficiently delivered using a multileaf collimator (MLC). Radiation may be delivered through a continuous (dynamic mode) or discrete (step-and-shoot) sequence of windows formed by the leaves. Algorithms and software that convert optimized intensity distributions into leaf trajectories apply approximate empirical corrections to account for the various effects associated with MLC characteristics, such as the rounded leaf tips, tongue-and-groove leaf design, leaf transmission, leaf scatter, and collimator scatter upstream from the MLC. Typically, the difference between inter- and intraleaf transmissions is ignored. In this paper, using a schematic example of IMRT for head and neck carcinomas, we demonstrate that complex anatomy and severe optimization constraints produce complex intensity patterns. Using idealized intensity patterns we also demonstrate that, for complex intensity patterns, the average window width tends to be smaller and, for the same dose received by the tumor, the number of MUs is larger. We found that as the complexity increases, so does the contribution of radiation transmitted through and scattered from the leaves (“indirect radiation”) to the total delivered dose. As a consequence, the lowest deliverable intensity in complex intensity patterns may be significantly greater than that required to provide adequate protection for some normal tissues. Furthermore, since corrections for leaf transmission and scatter effects are approximate and the difference between inter- and intraleaf transmission is ignored, the accuracy of the delivered dose may be affected. Using the results of a simple experiment and a typical intensity-modulated beam for a head and neck case as examples, we show the effect of window width and complexity on the accuracy and deliverability of intensity patterns. Some possible strategies for improving the accuracy and for relaxing the lower limit on deliverable intensity are discussed. © 2000 American Association of Physicists in Medicine. [S0094-2405(00)00306-0]

Key words: intensity-modulated radiotherapy, dynamic multileaf collimation

I. INTRODUCTION

The main purpose of the work presented in this paper is to investigate the impact of frequency and amplitude of fluctuations in intensity distributions on intensity-modulated radiotherapy (IMRT) dose distributions. We use the term “complexity” to subjectively describe the frequency and amplitude of fluctuations in the intensity distribution of a beam. The complexity of intensity distributions produced by IMRT optimization depends upon many factors. These include the shapes, sizes, and relative locations of tumor and normal tissues, the required tumor dose, dose homogeneity, and dose-volume limits of normal tissues. They may also include the choice of the objective function, grid size, and beam and collimator angles. We will demonstrate that more complex intensity patterns take longer (i.e., require more MUs) to deliver and, due to the contribution received from leaf transmission and scatter, impose a high lower limit on the minimum intensity received by a point, and may, therefore, negatively affect the quality and accuracy of dose distributions.

Intensity-modulated beams may be efficiently delivered using a multileaf collimator (MLC).^{1–7} The MLC may be used in the dynamic mode with a “sweeping window” technique, in which the leaves are continuously moving during irradiation, or in the “step-and-shoot” mode, in which the beam is off while the leaves move. In either case, radiation is delivered through a sequence of windows formed by the leaves. The intensity distribution of each beam, produced by an IMRT optimization system, which we call the “desired intensity distribution” here, is converted into optimum leaf trajectories as a function of monitor units. Approximate empirical corrections are applied to account for the various effects associated with MLC characteristics, such as the rounded leaf tips, tongue-and-groove leaf design, leaf transmission, leaf scatter, and collimator scatter upstream from the MLC. Generally, the difference between inter- and intraleaf transmissions is ignored.

The accuracy of delivered dose depends upon the adequacy of these corrections. For certain disease sites, head and neck (HN) carcinomas, for instance, the intensity pat-

terns tend to be highly complex. As a consequence, the average window width required to deliver such patterns is narrow. Therefore, each point within the beam aperture may receive a significant fraction of its intensity from indirect sources, i.e., transmission through and between the leaves, and scattering from the leaves, and not directly through the window. It is not uncommon for some of the points to receive 100% of their intensity indirectly. The large magnitude of indirectly received intensity can affect the quality of IMRT dose distributions in two different ways. First, the minimum deliverable intensity may be high and may limit the ability of IMRT to adequately reduce dose to normal structures. Second, since the corrections applied for leaf transmission and scattering are approximate, and since the difference between inter- and intraleaf transmissions is ignored, the accuracy of delivered dose may be compromised. Therefore, it is important to understand the causes of the complexity of intensity patterns, their effect on dynamic MLC (DMLC) window width, the number of MUs to deliver a treatment, the fraction of radiation received through transmission and scattering, and their potential impact on quality and accuracy. In this paper, we use a schematic example of IMRT for head and neck carcinomas to illustrate that complex anatomy and severe optimization constraints produce complex intensity patterns. We do not address the effect of the other factors mentioned above. A complete and thorough study of all factors would be better reported in a separate paper. Using idealized intensity patterns and a typical intensity-modulated beam of a head and neck case, we also demonstrate the impact of complexity on the window width, the number of MUs, and the fraction of indirectly received dose. We also show that, due to the approximate nature of corrections for the indirect contribution and the averaging of inter- and intraleaf transmission variation, the uncertainty in delivered dose for complex intensity patterns is increased.

There are several ways to reduce the complexity of intensity patterns and to minimize the contribution from indirect sources. Each method has its strengths and weaknesses. In this paper we discuss these briefly but illustrate only the use of a filtration technique to reduce the amplitude of intensity fluctuations and its effect on dose distributions and the number of monitor units. Subsequently, it would be important to thoroughly investigate this and other techniques to improve the quality and accuracy of IMRT.

II. METHODS AND MATERIALS

In this paper we assume that intensity distributions are delivered with a DMLC using the “sweeping window” technique. Using special algorithms and software, intensity distributions created by IMRT optimization systems are converted into trajectories of leaves to deliver desired dose distributions. Groups of leaf pairs are used to modulate intensities to produce two-dimensional nonuniform profiles of arbitrary shape. The window formed by each pair of opposing leaves sweeps monotonically across the target volume while the radiation beam is on. The window width opening and its speed are variable. Since the dose rate of the treat-

ment machine might fluctuate slightly, the motion is indexed to monitor units (MUs) rather than time. As the window sweeps across a point, the radiation dose received directly by the point is proportional to the number of MUs elapsed from the time the tip of the leading leaf (“*L* leaf”) goes past the point and exposes it until the tip of the following leaf (“*F* leaf”) moves in to block it again. The optimum setting of the window opening and its speed for each pair at any instant are determined by a technique first introduced by Convery and Rosenbloom,¹ with subsequent refinements by Bortfeld *et al.*,⁸ Spirou and Chui,^{4,9} Stein,⁵ Wang,⁶ and others. Knowledge of the maximum leaf speed is taken advantage of to maximize the gap between the opposing pairs of leaves and, therefore, to minimize the number of monitor units required for delivering the treatment.

Although the basic algorithm for converting intensity distributions into leaf trajectories is simple, it assumes that inter- and intraleaf transmission is zero, the tips of the leaves are focused at the radiation source and there is no tongue and groove effect. The actual leaf shape (we use the Varian 80 leaf MLC) is quite complex, and algorithms have been developed to approximately correct for leaf transmission and rounded tips. In addition to this, MLC scatter and the effect of the varying DMLC aperture on head scatter (i.e., the radiation scattered upstream from the MLC) needs to be accounted for.

Generally, the algorithms we use, described in the following subsections, are similar to those developed by Spirou *et al.* and Stein.¹⁰ However, there are several differences. The principal distinctions include the manner in which we compute the leaf transmission, determine transmission information for rounded leaf tips and incorporate head scatter. Also, our studies have shown that scattering from the MLC may be a significant fraction of the indirect radiation but is diffusely distributed in contrast with radiation transmitted through the leaves. We explicitly take these into account as two separate components.

A. Intensity distributions

Before proceeding with the description of algorithms to generate DMLC leaf sequences, we briefly describe the production of optimized nonuniform intensity distributions. We define the term “opening density” $\Omega(x,y)$ as the degree of “openness” of the DMLC as viewed from a point (x,y,z) in an arbitrary nonuniform field. [Coordinates (x,y) are in the “fanline” system, x being the direction parallel to leaf motion.] $\Omega(x,y)$ is that portion of the total “beam-on time” for which the point (x,y,z) is exposed to the source of the primary (direct) radiation unobstructed by dynamic leaves as the window formed by the leaves sweeps across the field. (The term “beam-on time” is used here not to describe the actual time but to describe the number of MUs for which the beam is on. We use the two terms interchangeably in this paper.) During beam on, the point will also receive radiation indirectly, i.e., transmitted through as well as scattered from the leaves. We define another quantity, the “effective” opening density $\Omega_e(x,y)$, which is the direct portion of the total number of monitor units, plus the indirect portion.

With this definition of opening density the direct portion $\Phi_d(x,y,z)$ of the fluence (intensity) $\Phi(x,y,z)$ at (x,y,z) , i.e., the portion originating at the source, is given by

$$\Phi_d(x,y,z) = \Omega_e(x,y) \times P(x,y,z), \quad (1)$$

where $P(x,y,z)$ is the primary portion of the unmodulated incident beam. The head-scattered portion of the fluence is given by an approximate expression

$$\Phi_s(x,y,z) = \{\Omega(x,y) \times P(x,y,z)\} \otimes s(x,y,z). \quad (2)$$

The symbol \otimes represents convolution and $s(x,y,z)$ characterizes scattering from the collimation system upstream, originating mostly from the flattening filter. Since the head scatter contributes only a relatively small fraction of the total delivered dose, we assume that $\Omega(x,y) \approx \Omega_e(x,y)$ in Eq. (2).

In a typical dose calculation system that adequately takes phantom-scattered radiation into account, a “dose-spread kernel” is convolved with the total incident fluence times the linear attenuation coefficient to predict dose in three dimensions as follows:

$$D(x,y,z) = \mu \times \{\Phi_d(x,y,z) + \Phi_s(x,y,z)\} \otimes k(x,y,z). \quad (3)$$

This type of model is implemented in our commercial treatment planning system (ADAC’s Pinnacle) and is used for dose distribution calculation in the IMRT optimization system developed by us.¹¹ It takes into account both the collimator scatter upstream from the MLC and the lateral transport of radiation to compute the dose accurately for surface irregularities, internal inhomogeneities, beam boundaries (penumbra), and arbitrary nonuniform intensity distributions. In a typical intensity-modulation optimization process, an opening density matrix $\Omega_e(x,y)$ in a plane through the isocenter and normal to the central axis is produced. The points along the direction of leaf motion (x direction) represent a row through the middle of each leaf. The grid size of the matrix along the y -axis is set equal to the width of the MLC leaf, and the grid size along the x -axis is as small as practical (1–4 mm). All matrix points outside the boundary of the beam’s eye view of the tumor, plus a margin for penumbra, are set to zero (or a low threshold value equal to the expected value of radiation transmitted through the leaves). During optimization it is assumed that the intensity distribution represented by the opening density matrix $\Omega_e(x,y)$ will be delivered, whether directly or indirectly. (The term opening density and intensity are used interchangeably in the rest of the paper.) In reality, the deliverable intensity matrix may be different for reasons that will become clear from the discussion in the following subsections.

B. Leaf sequence generation

The matrix $\Omega_e(x,y)$ is the desired opening density matrix. It is used to compute the leaf trajectories of the DMLC. The formalism we use is nearly identical to that of Spirou and Chui.^{4,9} We refer the reader to the references cited for details of the derivation but list some important equations for clarity of presentation.

For the moment, we ignore the radiation scattered from the leaves. We assume that radiation scattered from the MLC is a small fraction of the total intensity and is a diffusely distributed portion of $\Omega_e(x,y)$. An additive correction for it can be incorporated iteratively as described later in the next subsection. From known leaf trajectories and leaf transmission characteristics, the effective opening density value at a particular point i for the leaf pair is given by the expression

$$\Omega_e(x_i) = \int_0^M \tau_L(x(m) - x_i) \times \tau_F(x(m) - x_i) \times dm. \quad (4)$$

In this expression, $\tau_L(x(m) - x_i)$ and $\tau_F(x(m) - x_i)$ are “transmission functions” which represent the transmitted fraction of radiation at x_i as a function of the distance between the point x_i and the position $x(m)$ of the rounded leaf tips of the L and F leaves when m MUs have been delivered. The value of the transmission function is 1 when the point is not covered by either of the leaves. The leaf transmission function for a Varian MLC is shown in the next section. The integrand in Eq. (4) represents the number of MUs received by the point x_i for the beam-on time of dm . We have dropped the y argument in $\Omega_e(x,y)$ for simplicity. M is the total number of MUs for the beam. For the trivial case in which the transmission through the leaves is zero and the leaves are focused,

$$\Omega_e(x_i) = M_F(x_i) - M_L(x_i), \quad (5)$$

where $M_L(x_i)$ is the monitor unit reading when the L leaf tip exposes the point x_i and $M_F(x_i)$ is the reading when the F leaf covers it again. However, for a realistic case, a portion of the radiation received by a point is transmitted through the leaves. For the time being we continue to assume that the leaf tips are focused at the source and the transmission though the leaf is a constant τ . We will deal with rounded leaf tips later. Then, for $\Omega_e(x_{i+1}) > \Omega_e(x_i)$,

$$M_L(x_{i+1}) = M_L(x_i) + \frac{x_{i+1} - x_i}{v_{\max}} \quad (6a)$$

and

$$M_F(x_{i+1}) = M_L(x_{i+1}) + \frac{\Omega_e(x_{i+1}) - M \times \tau}{(1 - \tau)}, \quad (6b)$$

and for

$$\Omega_e(x_{i+1}) \leq \Omega_e(x_i), \quad (6c)$$

$$M_F(x_{i+1}) = M_F(x_i) + \frac{x_{i+1} - x_i}{v_{\max}},$$

and

$$M_L(x_{i+1}) = M_F(x_{i+1}) - \frac{\Omega_e(x_{i+1}) - M \times \tau}{(1 - \tau)}, \quad (6d)$$

where v_{\max} is the maximum permissible leaf velocity (in units of cm/MU). M is the total beam-on time, which is not known *a priori*. It is determined as follows. In order to deliver the treatment as rapidly as possible, at any one instant, one of the leaves of the pair must travel at its maximum

permissible velocity. Which leaf of the opposing pair should travel at its maximum speed depends upon whether the opening density is rising or falling from point i to point $i+1$. If $\Omega_e(x_{i+1})$ is greater than $\Omega_e(x_i)$, then the leading leaf must travel at v_{\max} [expressions 6(a) and 6(b)], otherwise the following leaf must travel at v_{\max} [expressions 6(c) and 6(d)]. We also assume that, at the start of the beam (MUs=0), both the L and the F leaves of the pair are positioned at their starting closed position. The starting position is the grid point just before the first nonzero element of the row of the opening density matrix. The beam-on time M^l for this leaf pair l is the MU value when the F leaf of the pair reaches its terminal position. The terminal position of the leaf pair is the grid point just after the last nonzero element. The beam-on time for this leaf pair is then given by (see Spirou and Chui for details of the derivation^{4,9})

$$M^l = (1 - \tau) \frac{x_{i_{\text{last}}} - x_{i_{\text{start}}}}{v_{\max}} + \sum_{\substack{i=i_{\text{start}} \\ \Omega(x_{i+1}) > \Omega(x_i)}}^{i_{\text{last}}-1} [\Omega_e(x_{i+1}) - \Omega_e(x_i)]. \quad (7)$$

Since all quantities on the right hand side are for the same leaf pair, we have omitted the superscript l . The contribution of the first term to the beam-on time is the same regardless of the intensity fluctuations, but the contribution of the second term depends upon the complexity of the opening density profile.

Let us consider a couple of simple examples to underscore the increase in beam on time when the complexity of the intensity pattern increases. Note that, due to the assumption that both leaves are at their closed position initially, $\Omega_e(x_{i_{\text{start}}+1}) > \Omega_e(x_{i_{\text{start}}})$ always. If $\Omega_e(x_i) \leq \Omega_e(x_{i-1})$ for all the remaining terms in the sum (i.e., the opening density is monotonically decreasing after the first rise), the beam-on time will be

$$M^l = (1 - \tau) \frac{x_{i_{\text{last}}} - x_{i_{\text{start}}}}{v_{\max}} + \Omega_e(x_{i_{\text{first}}+1}). \quad (8)$$

Similarly, if $\Omega_e(x_i) \geq \Omega_e(x_{i-1})$ for all the remaining terms (monotonically rising opening density), the beam-on time is given by

$$M^l = (1 - \tau) \frac{x_{i_{\text{last}}} - x_{i_{\text{start}}}}{v_{\max}} + \Omega_e(x_{i_{\text{last}}}). \quad (9)$$

That is, for a beam for which the opening density is increasing or decreasing monotonically, the beam-on time depends upon the peak value of the opening density and is independent of the values at the intermediate points. However, if the opening density falls and then rises for some of the points, the beam-on time will increase depending upon both the frequency and the amplitude of the fluctuations.

The total beam-on time M is the maximum of the beam-on times of individual leaf pairs. That is,

$$M = \max\{M_{ij}\}. \quad (10)$$

This is the value when the slowest leaf pair reaches its terminal position and the beam goes off. Note that the value of

M computed in this manner is an approximation (but a good one) since the rounded tips of the leaves and MLC scatter have not yet been taken into account.

Using this value of beam-on time M , an approximate trajectory is calculated using Eqs. 6(a)–6(d). More accurate trajectories and beam-on time are calculated iteratively. Such calculations require an accurate knowledge of the leaf transmission function and MLC scatter.

C. Estimation of rounded leaf tip transmission and MLC scatter

In principle, the transmission function can be computed analytically with the knowledge of the shape of the leaf tip and the energy spectrum. We have used the Monte Carlo-generated energy spectrum for our treatment machine (Varian Clinac 2100C) for such computations. We have also experimentally obtained the contribution of MLC scattering as a function of blockage of the field by the MLC. In addition, we have used direct Monte Carlo simulations to independently confirm MLC transmission and scatter data. The Monte Carlo simulations take into account the finite size of the source at the bremsstrahlung target. Our work on the determination of the rounded leaf tip transmission function and MLC scatter is being reported elsewhere.¹²

Our measurements and Monte Carlo calculations show that, for a field completely blocked by the MLC, the MLC scatter is a very slowly varying function of position in the field and is proportional to the field size defined by the jaws, i.e., to the surface area of the MLC exposed to the direct beam.¹² The MLC scatter contribution to a point i for leaf pair l is then proportional to the average of the number of MUs for which each of the intensity matrix points is blocked and is given by

$$M_{S_{\text{MLC}}}(x_i, y_l) = S_{\text{MLC}}(L \times W) \times M_{\text{blocked}}^{\text{av}}, \quad (11)$$

where $S_{\text{MLC}}(L \times W)$ is the MLC scatter contribution per MU for an $L \times W$ field completely blocked by the MLC and

$$M_{\text{blocked}}^{\text{av}} = \frac{1}{N} \sum_l \sum_i M_{\text{blocked}}(x_i, y_l). \quad (12)$$

Here N is the number of intensity matrix points bounded by jaws. $M_{\text{blocked}}(x_i, y_l)$ is the number of MUs for which the intensity matrix point (x_i, y_l) is blocked, which is the difference between the total beam on time M and $M_{\text{open}}(x_i, y_l)$, the effective monitor units received by the point directly through the MLC window openings. The quantity $M_{\text{open}}(x_i, y_l)$ is also calculated using expression (4) but assuming that the leaf transmission function is a step function, i.e., the transmission is one when the point is within the leaf gap and zero if it is shadowed by one or the other leaf.

D. Iterative incorporation of rounded leaf tip transmission and MLC scatter

The resulting leaf transmission function and MLC scatter data are utilized in the conversion of intensity distributions into leaf trajectories as follows. The method we use is a modification of an iterative method of accounting for

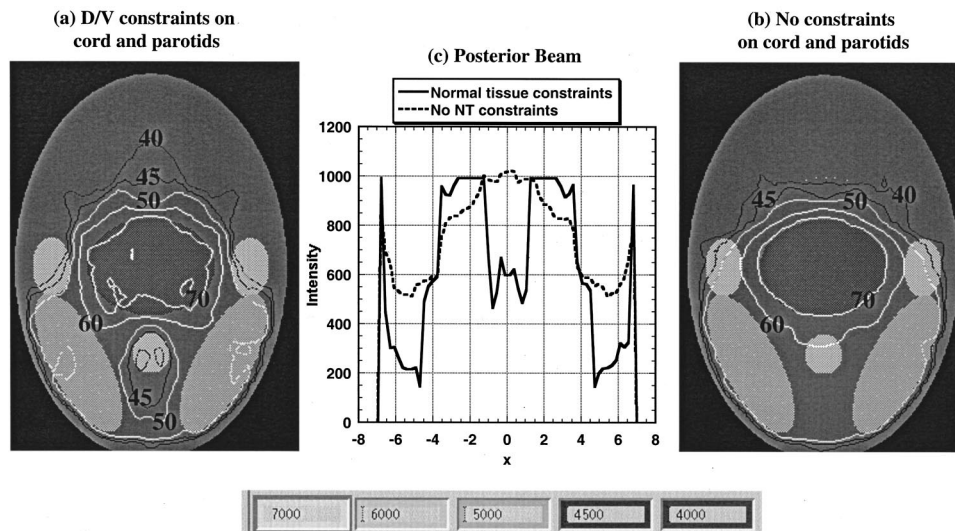


FIG. 1. Two 9-beam, 6 MV IMRT plans illustrating the effect of complexity of anatomy and severity of constraints on the complexity of intensity distributions.

rounded leaf tips suggested by Spirou⁴ and Stein.⁵ We first compute approximate leaf trajectories assuming constant leaf transmission and ignoring rounded tips and MLC scatter based on expressions 6(a)–6(d). The result is a table of MUs as a function of the position of each of the leaves of the pair. One such pair of tables is computed for each leaf pair participating in the treatment. These tables are then inverted to compute leaf trajectories in the form of leaf positions as functions of MUs. Using these approximate trajectories, we next compute the opening density matrix that will actually be generated. This is accomplished by integrating the leaf transmission function for each leaf pair over the total beam-on time using expression (4). To each point, we also add the contribution of scatter from interactions occurring in the MLC.

These calculations produce a new opening density matrix. Let us denote this opening density matrix by $\Omega_{e,1}(x,y)$. The input opening density matrix for the next iteration is then changed by the difference between the desired $\Omega_e(x,y)$ and the computed opening density matrix $\Omega_{e,1}(x,y)$. In the next iteration, a new opening density matrix $\Omega_{e,2}(x,y)$ is computed. These steps are repeated until convergence is achieved; in our experience, this takes no more than five iterations. The resultant opening density matrix is not exactly the same as $\Omega_e(x,y)$ but is the closest approximation achievable due to the fact that a portion of the radiation is received through transmission and scattering. We call it the “deliverable” opening density $\Omega_e^d(x,y)$. The leaf trajectories which produced $\Omega_e^d(x,y)$ (i.e., the last iteration trajectories) are used to deliver the treatment. This process also yields the MU values when each of the F leaves comes to a stop, and the MU setting for the beam as a whole is equal to the largest of the individual leaf pair MU values.

In the discussion above, we have assumed that there is no variation in transmission normal to the direction of leaf motion. In reality, measured transmitted dose has been found to vary from 1.3% to 2.1%.¹² We ignore this variation and use an average transmission of about 1.7%. If a large fraction of the radiation dose in a region is received via transmission,

this variation may not be negligible. We will discuss the potential consequences of this approximation in the next section.

III. RESULTS AND DISCUSSION

Figure 1 is an illustrative example that demonstrates how the complexity of the anatomy and the severity of constraints can affect the complexity of intensity distributions. A schematic HN phantom with a centrally-located tumor volume, nodes, parotid glands, and spinal cord was used. Two 9-beam IMRT plans were developed. In both plans, the primary tumor was prescribed 70 Gy, and the nodes were prescribed 50 Gy each. In plan (a) the spinal cord was constrained to receive no more than 45 Gy, and 50% of the volume of the parotids was constrained to receive no more than 30 Gy. In addition, a low priority dose constraint was imposed on nonspecific normal tissues so as not to compromise the dose to the tumor and nodes. In plan (b) the constraints on the spinal cord and parotids were removed. Figure 1(c) compares the optimized intensity profiles in the transverse-plane through the isocenter for the posterior beam for the two cases. For the case with constraints, there is a valley in the middle to limit the cord dose. In addition, there are two deep valleys just inside the boundaries of the beam mainly to reduce the dose to the parotids while delivering some dose to the nodes. The sharp peaks at the edges of the beam are due to an inherent characteristic of IMRT optimization, which is that it sharpens beam boundaries by depositing additional fluence to compensate for the lateral transport of radiation.^{13,14} For the case without constraints, the central valley disappears, and the two valleys on either side of the center are much shallower. They are still there since the desired dose to the nodes is lower than that to the target volume. Similar reductions in the complexity of intensity patterns of other beams were found.

Figures 2(a)–2(f) illustrate the effect of intensity fluctuations on the number of monitor units. We classify the intensity patterns in Figs. 2(a) and 2(b) as simple, 2(c), 2(d), and

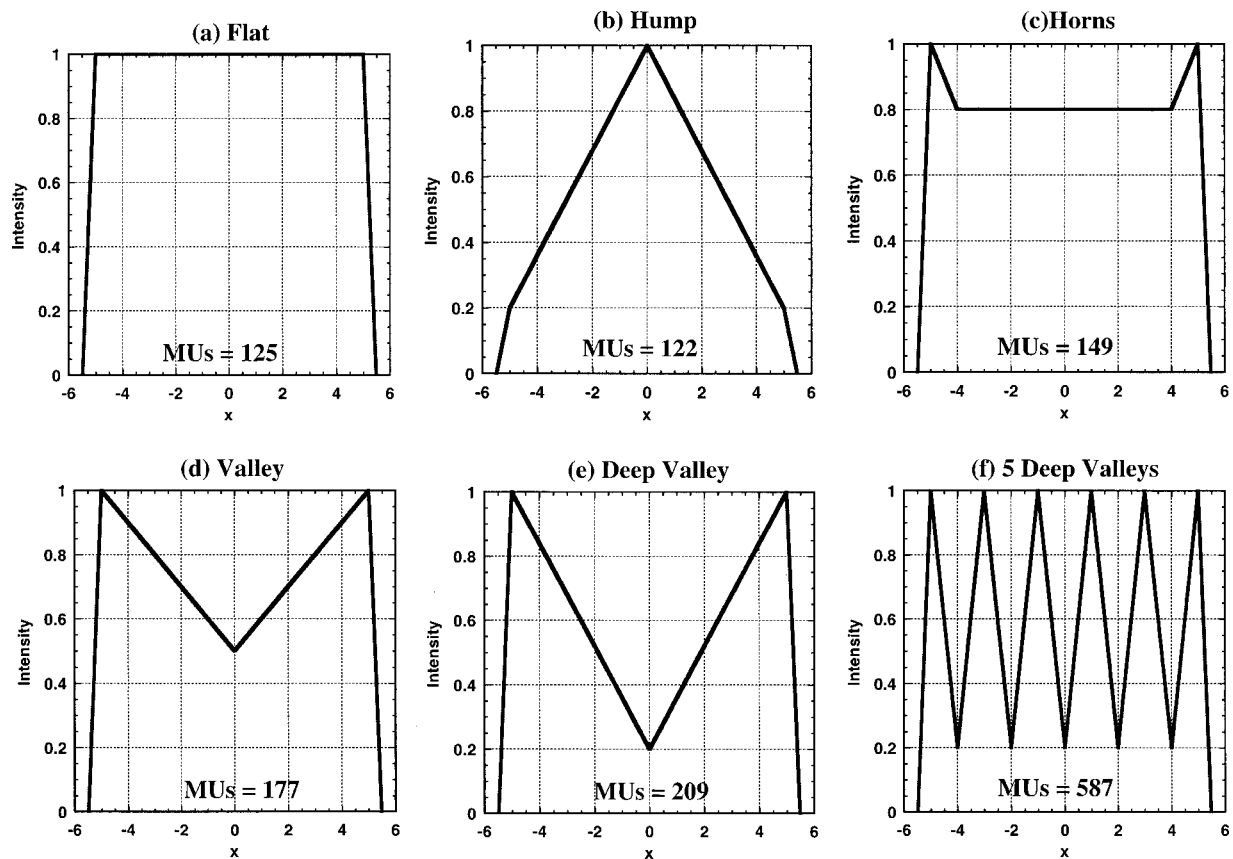


FIG. 2. Beam-on time (MU settings) needed to effectively deliver 100 MUs peak value (corresponding to an intensity of 1) for the intensity patterns shown. Calculations were done using the sliding window technique, a maximum leaf speed of 2 cm/s and a dose rate of 240 MU/min. Corrections for leaf transmission and rounded leaf tip were included.

2(e) as moderately complex, and 2(f) as the most complex (many deep valleys). In each case the peak intensity is unity. The monitor unit settings required to deliver 100 MUs effectively at the peak with the sliding window technique were calculated using formalisms presented in the previous section. The effects of leaf transmission, rounded leaf tips and scattering from the MLC were included. In all cases, each leaf pair was assumed to be positioned at the left edge of the field at the start of irradiation. A leaf speed of 2 cm/s and a dose rate of 240 MU/min were used for these calculations. The calculated MU settings are shown on the figures themselves. It should be noted that the grid size at which the intensities were specified is 0.5 cm. This explains the sloping boundaries. As may be intuitively obvious, and is clear from figures (b)–(f), the number of MUs required to deliver the same maximum intensity increases as the amplitude (depth of valleys) and the frequency (number of valleys) of fluctuations increases.

Figure 3 shows leaf trajectories [MUs vs leading (L) and following (F) leaf positions] for the three different desired intensity patterns shown above them. For the 10-cm wide uniform field [Fig. 3(a)], the L leaf moves at the maximum speed to a point near the right edge of the field. Both leaves then move very slowly while most of the dose is delivered. The F leaf then moves at the maximum speed while the remaining few MUs are delivered. The vertical distance be-

tween the two curves at any point on the x -axis, plus the fluence received through transmission and scattering, should be equal to the desired intensity. The window width during this period (except at points near the field edges) is 10 cm. For the moderately complex pattern of Fig. 3(b), the sweeping window width increases from its initial closed position to a maximum of approximately 6.5 cm and varies from nearly 5.5 cm to 6.5 cm before closing again. The number of MUs required to deliver such a pattern is nearly doubled. In the most complex pattern, shown in Fig. 3(c), the window width increases from its closed position to a maximum of approximately 1 cm and varies from the maximum value at the peak intensity to zero at the minimum intensity. This means that all of the intensity at the minimum (20%) of the intensity pattern is received indirectly through leaf transmission and scattering. Figure 4 shows the contribution of the direct and indirect portions at each point along the intensity profile. For the moderately complex pattern of Fig. 4(a), the indirectly received intensity varies from approximately 8% to about 11% of the maximum intensity. The anomalies at the field boundaries are mainly due to the large grid size chosen for the purposes of these illustrations. Also note that the intensity outside the intensity-modulated field boundary is set to zero due to the presence of jaws, which are assumed to block all the radiation. For the complex pattern, the indirect contribution varies from approximately 20% to 40% of the

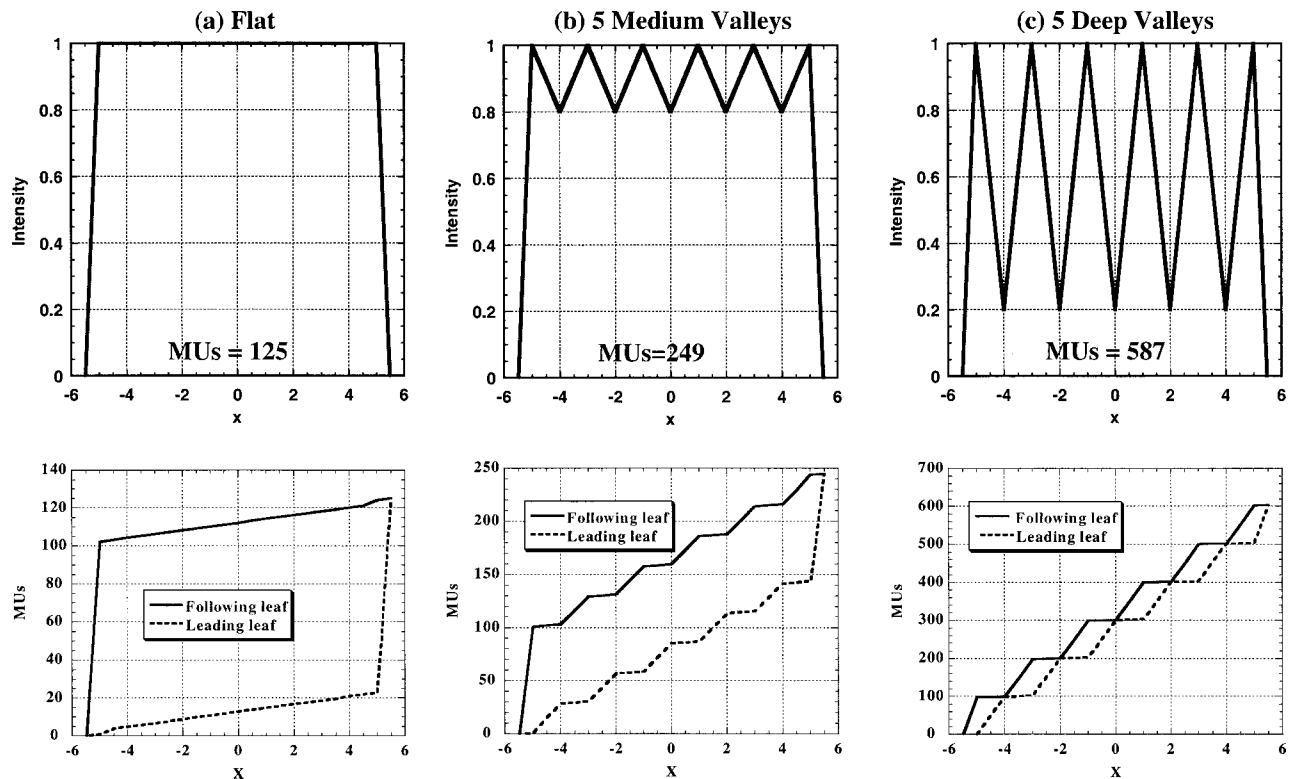


FIG. 3. Dependence of leaf trajectory and window width on the fluctuations of the intensity pattern.

maximum, or from 100% to 40% of the local intensity value. In summary, for highly complex intensity patterns, a large fraction of intensity at a point may be received indirectly. In fact, as pointed out earlier in the paper, and as we shall see in the clinical example below, in some complex intensity patterns, the optimized intensity at some points may be too low to be deliverable due to a limitation imposed by the contribution from leaf transmission and scattering.

We also experimentally estimated the magnitude of the indirect contribution as a function of window width and its effect on the accuracy of delivered dose. A series of 10 cm \times 10 cm uniform intensity test fields were generated dy-

namically with sweeping windows formed by pairs of opposing leaves with fixed separations ranging from 0.5 cm to 10 cm. Each of these trajectories was designed to deliver 100 MUs of direct fluence to the 10 \times 10 cm² fields. The total MUs needed ranged from 180 to 2100 (column 3 of Table I). Thus, for ideal leaves (double focused, no transmission, and no leaf scatter), each trajectory should deposit 100 cGy at the calibration point. In reality, each field received additional dose through transmission and scatter. Column 4 shows the ratio of actual measured dose to the dose expected for idealized leaves. Measurements were made with calibrated film, and measured values shown are an average normal to the

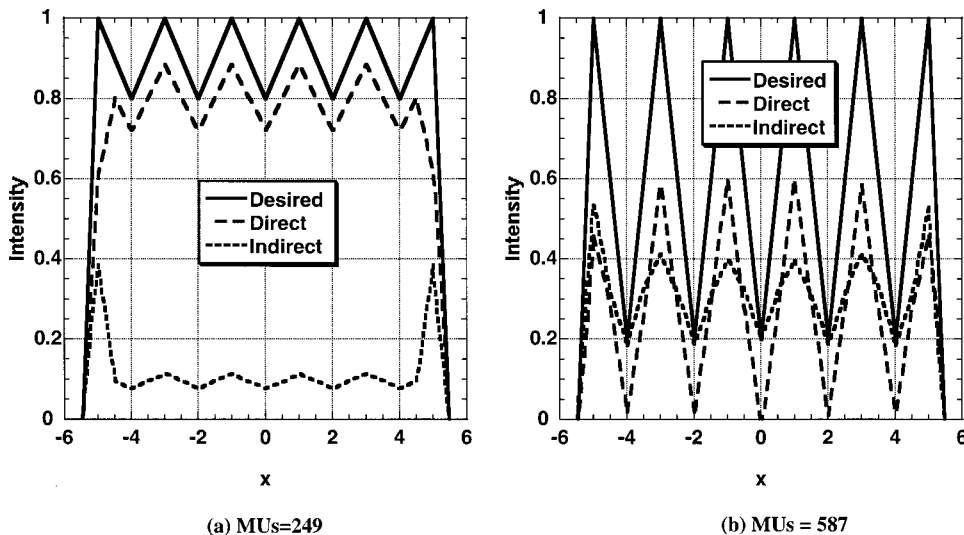


FIG. 4. Contributions from direct and indirect sources (transmission through the leaf and the rounded leaf tip and MLC scatter) as a function of the fluctuations in intensity patterns.

TABLE I. Measured and calculated doses on the central axes of 6 MV, 10 cm×10 cm, “uniform” beams generated dynamically with varying window widths ranging from 0.5 cm to 10 cm. Measurements shown were done with calibrated films. The dose rate for the measurements was 240 MU/min. The dose values shown were averaged for inter- and intraleaf leakage.

Dose relative to 10 cm×10 cm open fixed field												Discrepancy %		
1. Window width (cm)	2. Leaf velocity (cm/s)	3. MU settings to deliver 100 cGy with ideal leaves	5. Calculated dose corrected for leaf transmission							6. Calculated dose corrected for leaf transmission and MLC scatter			7. Measured MC-corrected	8. Measured MC-corrected +leaf shift
			4. Measured	a. Analytic transmission			b. MC-based transmission		c. MC-based transmission		c. MC-based transmission +leaf shift			
				a. Analytic transmission	b. MC-based transmission	c. MC-based transmission +leaf shift	a. Analytic transmission	b. MC-based transmission						
0.5	0.033	2100	1.740	1.448	1.490	1.610	1.576	1.618	1.738	7.01	0.11			
1	0.067	1100	1.376	1.224	1.245	1.304	1.288	1.309	1.368	4.87	0.58			
2	0.133	600	1.191	1.112	1.123	1.152	1.144	1.155	1.184	3.02	0.59			
3	0.2	432	1.125	1.069	1.076	1.096	1.090	1.097	1.117	2.47	0.69			
4	0.267	348	1.089	1.046	1.053	1.065	1.062	1.069	1.081	1.85	0.75			
5	0.333	300	1.084	1.045	1.049	1.061	1.058	1.062	1.074	2.05	0.94			
7	0.467	244	1.072	1.043	1.044	1.052	1.052	1.053	1.061	1.75	1.01			
10	0.667	180	1.029	1.018	1.020	1.025	1.023	1.025	1.030	0.38	−0.11			

direction of leaf motion. That is, the difference between inter- and intraleaf transmissions has been averaged. The contribution from indirect sources is the highest for the narrowest window, varying from 74% of the expected value for the 0.5 cm window width to 2.9% for the 10 cm wide window. Columns 5(a) and 5(b) show the calculated dose with corrections for transmission and scatter. The leaf transmission function for calculations shown in column 5(a) was obtained analytically, and the one for column 5(b) was based on Monte Carlo simulations.^{12,15} Figure 5 shows the two functions. The difference between the two curves is presumably due to the finite size of the source at the bremsstrahlung target. These data were averaged for inter- and intraleaf transmission.

In columns 6(a) and 6(b) the contribution of fluence scattered from the MLC was added. We notice that the calculated values with leaf transmission data based on Monte Carlo simulations and with MLC scattering included are closest to the measured values. However, discrepancies remain which range from 0.38% for the 10 cm wide window to 7.01% for the smallest window (column 7). The residual discrepancy may be due to one of several sources including the approximations in correction for leaf transmission, averaging of inter- and intraleaf transmissions, beam hardening, inaccuracies of film dosimetry, and possible imprecision in leaf positions. These sources need to be investigated further. In any case, there is a pattern that the discrepancy increases as the window width decreases. For the time being, we have assumed that the residual discrepancy is due to imprecision in leaf positions. We estimated that an outward shift of approximately 0.3 mm (projected to isocenter) in the position of each leaf relative to its nominal position will explain most of the discrepancy for the smallest window. Columns 5(c) and 6(c) show the data with the 0.3 mm leaf-shift correction applied. Column 8 shows that the agreement between measured and calculated values is significantly improved. (Interestingly, later measurements with a gauge revealed an outward shift in leaf positions of approximately 0.4 mm projected to the isocenter.)

As mentioned above, the data shown in Table I were averaged over intra- and inter-leaf transmissions. For actual clinical cases, depending upon the fractional dose received through transmission, the delivered dose may vary significantly due to differences between inter- and intraleaf transmissions. Figure 6 shows the plots of measured dose profiles perpendicular to the leaf motion direction for some of the beams included in Table I. It is seen that the variation in dose due to inter- and intraleaf transmission differences is small for window widths of 3 cm or larger but may be quite significant for smaller windows. For example, for the 0.5 cm window, the variation around the average is approximately $\pm 6\%$. In a typical clinical intensity pattern, the average window width may be 2–4 cm. However, window widths at different points of the trajectories may be much smaller.

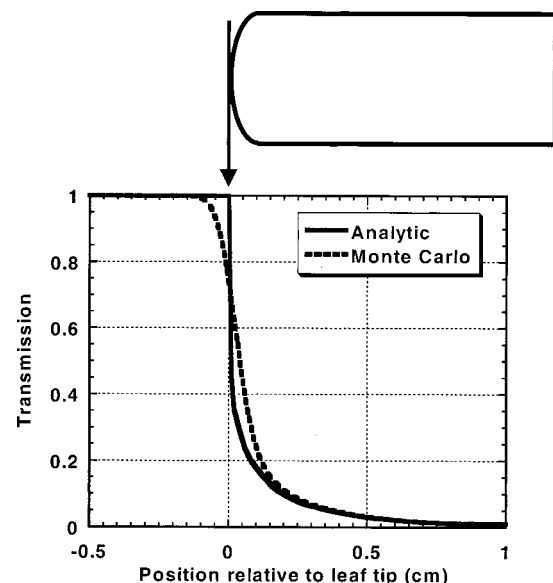


FIG. 5. Leaf transmission curves calculated analytically using the Monte Carlo-generated energy spectrum and by direct Monte Carlo simulations. The difference is ostensibly due to the finite size of the source spot at the bremsstrahlung target.

Interleaf leakage contribution as a function of window width

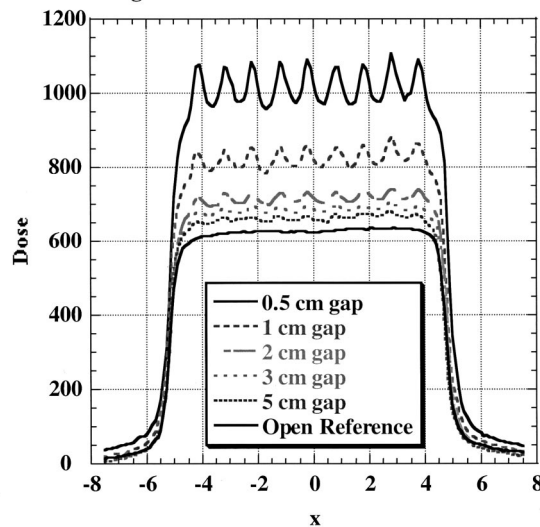


FIG. 6. Dose profiles, at the depth of maximum dose, perpendicular to the leaf motion direction of 10 cm×10 cm fields generated dynamically with window widths of varying sizes.

Therefore, the use of the average of inter- and intraleaf transmission could significantly affect the accuracy of dose at these points.

Table II shows the monitor units required for delivering the intensity profiles of the leaf pairs participating in the posterior beam of a 9-beam IMRT plan of a head and neck case. The peak effective MU value in the two-dimensional intensity pattern was 42. The MU values shown in the table resulted from the iterative procedure to calculate leaf trajectories described in Sec. II D. The second column is for the desired intensity profiles produced by IMRT optimization (the unfiltered profiles), and the third column is for profiles obtained by filtering the desired profiles to smooth out the high frequencies. Filtration was performed by convolving the Savitzky–Golay filter¹⁶ with the original profiles. The parameters of filtration were adjusted by trial-and-error so as to minimize the loss of relevant detail.

Filtration reduces the MUs required for all leaf pairs but by different ratios. The difference in ratios is presumably due to the difference in complexity of unfiltered profiles. Leaf pair 4 requires the largest number of MUs (263) for unfiltered intensity profiles, and leaf pair 6 required the largest number of MUs (130) for filtered profiles, a factor of 2 reduction in beam-on time. Arbitrarily, we have chosen leaf pair 6 for the following discussion. Figure 7(a) compares the unfiltered and filtered desired intensity profiles of this leaf pair. Figure 7(b) compares the unfiltered desired profile with the corresponding deliverable profile. The deliverable profile $\Omega_e^d(x, y)$ is computed using the leaf trajectories obtained by the conversion of the desired opening density matrix $\Omega_e(x, y)$ (see Sec. II). Figure 7(c) compares the filtered desired intensity profile with the corresponding deliverable filtered profile. The most noteworthy feature of these data is that for the filtered intensity profiles [Fig. 7(b)], in the region between $x=1.3$ cm–2.2 cm where the optimization process

TABLE II. Monitor units required for delivering trajectories generated from unfiltered and filtered intensity profiles of the posterior beam of a 9-beam head and neck IMRT plan. Only active leaves are listed. The maximum of the leaf pair MUs is the number of MUs required to deliver the beam as a whole.

Leaf pair	MUs for unfiltered trajectory	MUs for filtered trajectory
2	102.0	70.2
3	144.3	109.1
4	262.8	111.9
5	232.8	108.3
6	259.4	129.8
7	106.9	63.8
8	122.5	74.2
9	123.4	76.9
10	153.0	115.6
11	163.3	114.8
12	132.7	91.3
Max (“beam-on time”)	262.8	129.8

requires dose to be low, the deliverable values are significantly higher than the original desired values. In contrast, the deliverable filtered profile [Fig. 7(c)] is much closer to the profile obtained by the filtration of the desired profile and provides a significant improvement in the sparing of the normal structure. This difference is due to the reduction in the total number of MUs required to deliver the beam; this reduction decreases the indirect contributions of transmission and MLC scattering.

Using the unfiltered and filtered intensity distributions of this beam and the corresponding deliverable intensity distributions, dose distributions were calculated at a depth of 5 cm in a flat homogeneous phantom with its surface at a distance of 95 cm from the source. The dose kernel superposition algorithm of our treatment planning system (ADAC Pinnacle) was used. Figure 8 displays the dose profiles under the trajectories of leaf pair 6. Generally, as seen from Fig. 8(a), the smearing caused by the lateral transport of radiation diminishes the differences between the desired unfiltered and filtered dose profiles. One minor exception is the dose peak at about $x=1$ cm; it highlights the potential pitfalls of filtration and the caution one must observe in its use. The discrepancy at this position may be explained by noting that the filtration process merged two adjacent peaks in the intensity pattern into a single peak [see Fig. 7(a)].

An examination of Figs. 8(b) and 8(c), and their comparison with Figs. 7(b) and 7(c), reveals that, while the smearing caused by the lateral transport reduced the difference between the filtered dose profile and the corresponding deliverable dose profile, this is not necessarily so for unfiltered dose profiles. In particular, in the region between $x=0$ and 2 cm the difference is increased.

It should be noted that, although filtration may alter the dose distribution somewhat compared to the original optimized dose distribution and the deliverable dose distribution may be different from the optimized dose distribution, the decisions regarding prescription dose and doses to normal

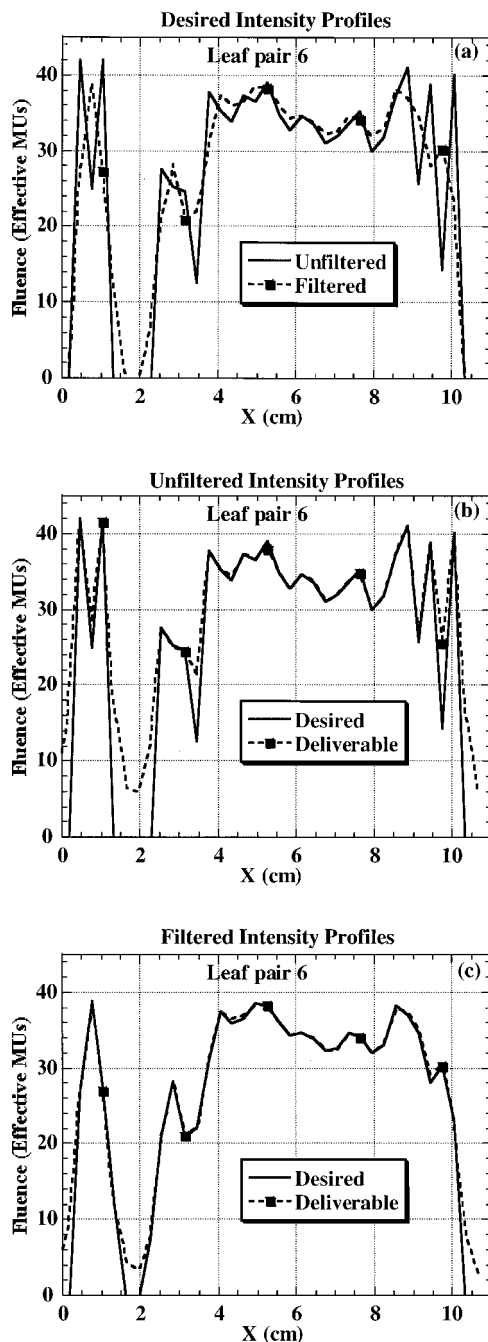


FIG. 7. Intensity profiles of the leaf pair that requires the largest number of MUs for the posterior beam of a 9-beam IMRT plan of a head and neck case. (a) compares the desired profile resulting from the IMRT optimization process (unfiltered profile) with the corresponding filtered profile. The MUs required to deliver unfiltered and filtered profiles were 263 and 130 respectively. (b) compares the unfiltered desired profile with the corresponding deliverable profile. The latter is generated during the conversion of the unfiltered intensity profile into leaf trajectories using the process described in Sec. II. (c) compares the filtered desired intensity profile with the corresponding deliverable profile.

structures are based solely on the filtered deliverable dose distributions and not on the original optimized dose distributions. Nevertheless, it is important to minimize the differences between the optimized and deliverable dose distributions so that the treatment delivered is nearest to the IMRT optimized distribution.

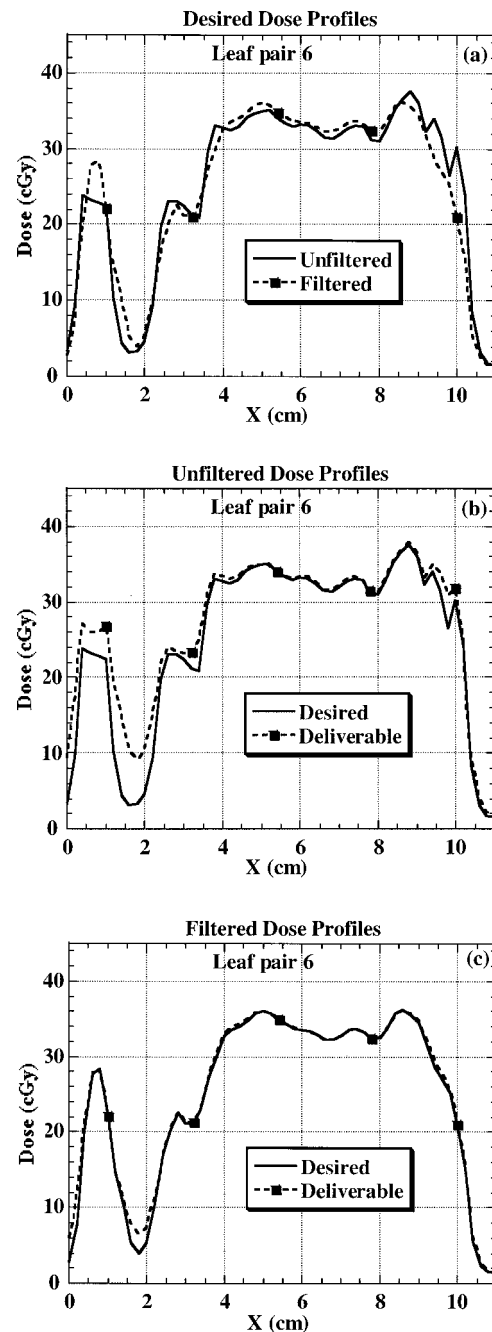


FIG. 8. A comparison of the calculated dose profiles corresponding to the intensity profiles shown in Fig. 7.

Figure 9 compares calculated deliverable and measured ("delivered") dose profiles for the same leaf pair for both unfiltered and filtered intensity distributions. The monitor units to deliver unfiltered dose distributions were 263 and to deliver filtered dose distributions were 130. While the agreement between calculated and measured dose profiles appears to be better for filtered data [Fig. 9(b)], the discrepancies in unfiltered dose profiles are relatively small, indicating the suitability of our methods and parameters to correct for leaf leakage.

Figure 10 displays the DVHs for the tumor, spinal cord, and the right parotid for the 9 beam head and neck treatment

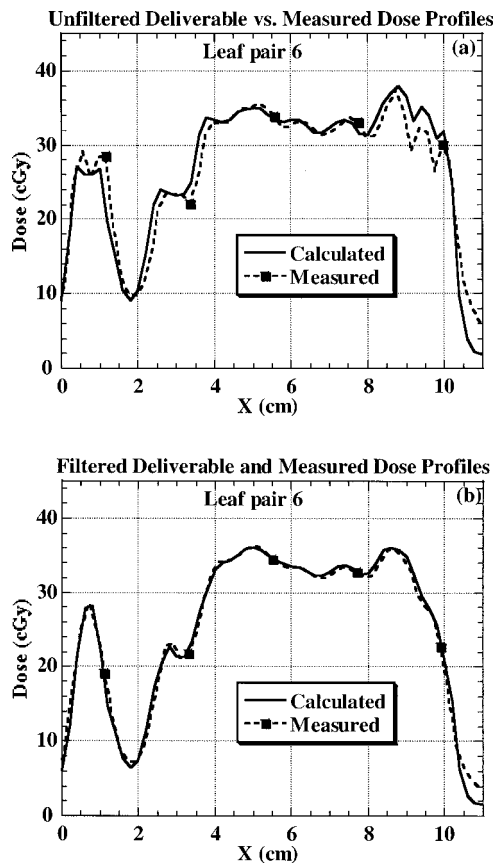


FIG. 9. A comparison of calculated deliverable dose profiles with the measured profiles for unfiltered and filtered intensity distributions.

plan illustrating the impact of filtration on desired and deliverable dose distributions. All dose distributions were normalized to deliver the same dose to 95% of the target volume. Tumor DVHs are essentially identical. Figure 10(a) shows that the deliverable dose distributions for both the spinal cord and parotids are significantly higher than the desired dose distributions. In other words, because of the MLC leakage, normal tissues receive higher dose than what the results of optimization may suggest. Figure 10(b) indicates that filtration has negligible impact on the desired dose distributions although the beam-on time, and hence the leakage, is considerably reduced. There is a slight increase in the spinal cord volume receiving dose between 22–28 Gy. Figures 10(c) and 10(d) demonstrate that filtration significantly reduces the gap between the desired and deliverable distributions and improves parotid and cord sparing.

In addition to filtration, the choice of grid size was examined to study its effect on the number of monitor units required and the corresponding effect on deliverability. We found that when the grid size along the motion of leaves is increased from 2 mm to 4 mm, the fluctuations in intensities decrease. For the patient whose data are shown in Figs. 6–10, we found that the number of monitor units to deliver the same set of beams were reduced by a factor of approximately 1.5. We chose a grid size of 3 mm for the treatment of this patient. The data shown in this paper were obtained using a grid size of 3 mm.

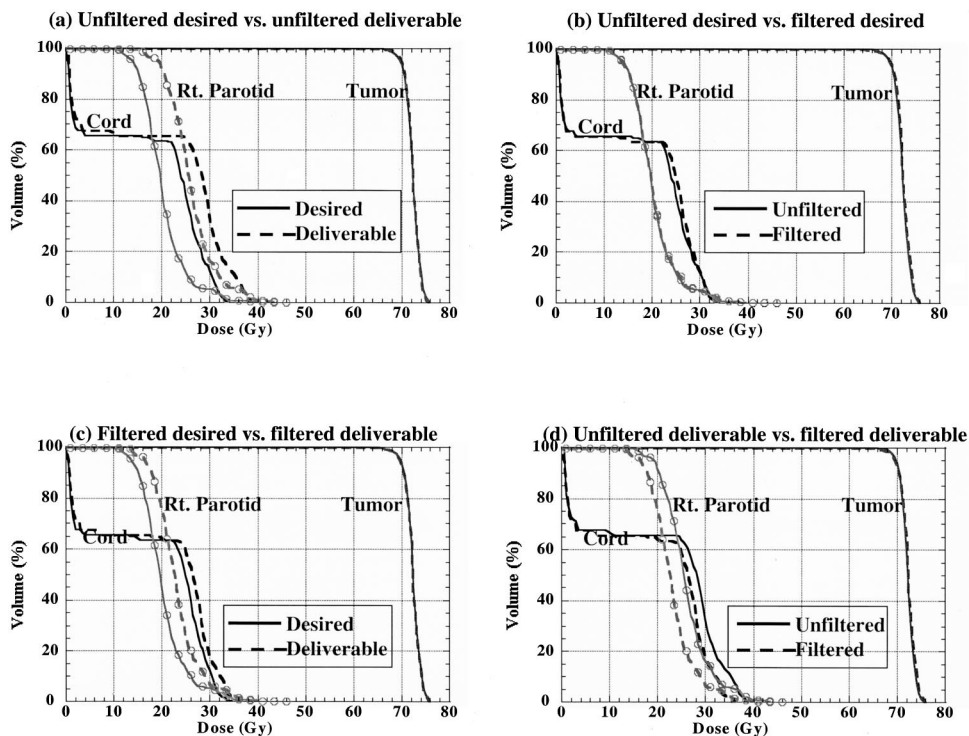


FIG. 10. Intercomparison of dose-volume histograms for the various combinations of unfiltered desired, filtered desired, unfiltered deliverable, and filtered deliverable dose distributions for the tumor, spinal cord and right parotid for the head and neck case.

IV. CONCLUDING REMARKS

There are several possible reasons for the complexity of intensity patterns. In this paper, using a schematic example, we demonstrated that complex anatomy and severe constraints lead to complex intensity patterns. The average window width required to deliver complex intensity patterns with the dynamic MLC is small, and the number of MUs is large. The window width at certain points may be much smaller than the average. For small window widths, the contribution to dose at a point from indirect sources (transmission through and scattering from the MLC) may be high. This has two negative consequences. First, the deliverable dose cannot be below the dose received indirectly and thus may limit the ability of the IMRT to provide the level of protection to normal tissues that it is, in principle, capable of. Second, since corrections for the indirect contribution are approximate and the difference in inter- and intraleaf transmissions is ignored, the uncertainty in dose for complex intensity patterns is increased.

Solutions to these problems are possible. We illustrated the use of a filtration technique to reduce fluctuations and reduce the number of MUs to deliver the same target dose distribution. We also found that increasing the grid size reduces fluctuations and the number of MUs. These steps allow a reduction in MLC leakage, the lowering of the doses to normal tissues where so required and, conceivably, an improvement in accuracy. However, caution must be observed in the use of these techniques since they may also reduce or remove useful parts of the intensity distributions.

There are other avenues that could be explored for reducing indirect contributions. Examples include thicker leaves, which would reduce leaf transmission, and a smaller interleaf gap, which would reduce the average transmission. Another way to reduce the leaf transmission would be to allow both pairs of jaws to continuously enclose the dynamically changing aperture. This step would require the jaws to move across the midline through substantial distances. In addition, the changes in in-air output factors as a function of jaw positions would need to be taken into account. Yet another way may be to optimize the collimator angle for each beam in order to find orientations which minimize fluctuations. This is possible but not trivial. It should be pointed out that all of these steps have strengths and weaknesses. None of them by itself would solve the problems fully, and a combination of methods is likely to be required.

In addition, to ensure that the delivered dose distributions accurately reflect the deliverable dose distributions calculated by the treatment planning system, it is important to understand the sources of indirect radiation, to estimate their

contributions accurately, and apply corrections for them using accurate algorithms. This work is especially important for IMRT of complex anatomical sites, such as head and neck.

ACKNOWLEDGMENTS

This work is supported by Grants Nos. CA74043 and CA74158 from the National Cancer Institute.

^{a)} Author to whom correspondence should be addressed. Tel: 804-828-8451; Fax: 804-828-6042; electronic mail: rmohan@hsc.vcu.edu

¹ D. J. Convery and M. E. Rosenbloom, "The generation of intensity modulated fields for conformal radiotherapy by dynamic collimation," *Phys. Med. Biol.* **37**, 1359–1374 (1992).

² J. M. Galvin, X. Chen, and R. M. Smith, "Combining multileaf fields to modulate fluence distributions," *Int. J. Radiat. Oncol. Biol. Phys.* **27**, 697–705 (1993).

³ L. Ma, A. Boyer, L. Xing, and C.-M. Ma, "An optimized leaf-sequencing algorithm for beam intensity modulation using dynamic multileaf collimators," *Phys. Med. Biol.* **43**, 1629–1643 (1998).

⁴ S. V. Spirou and C. S. Chui, "Generation of arbitrary fluence profiles by dynamic jaws or multileaf collimators," *Med. Phys.* **21**, 1031–1041 (1994).

⁵ J. Stein, T. Bortfeld, B. Doerschel, and W. Schlegel, "Dynamic x-ray compensation for conformal radiotherapy by means for multileaf collimation," *Radiother. Oncol.* **32**, 163–173 (1994).

⁶ X. Wang, S. Spirou, T. LoSasso, C. S. Chui, and R. Mohan, "Dosimetric verification of an intensity modulated treatment," *Med. Phys.* **23**, 317–328 (1996).

⁷ P. Xia and L. J. Verhey, "Multileaf collimator leaf sequencing algorithm for intensity modulated beams with multiple static segments," *Med. Phys.* **26**, 1424–1434 (1998).

⁸ T. Bortfeld, D. L. Kahler, T. J. Waldron, and A. L. Boyer, "X-ray field compensation with multileaf collimators," *Int. J. Radiat. Oncol. Biol. Phys.* **28**, 773–730 (1994).

⁹ S. V. Spirou, J. Stein, T. LoSasso, Q. Wu, R. Mohan, and C. S. Chui, "Incorporation of the source distribution function and rounded leaf edge effects in dynamic multileaf collimation (abstract)," *Med. Phys.* **23**, 1074–1074 (1996).

¹⁰ J. Stein, "Investigations on intensity-modulated treatment techniques in conformal radiotherapy," Ph.D. thesis Heidelberg, Germany, 1997.

¹¹ Q. Wu and R. Mohan, "Algorithms and functionality of an IMRT optimization system," *Med. Phys.* **27**, 701–711 (2000).

¹² M. R. Arnfield, J. V. Siebers, J. O. Kim, Q. Wu, P. J. Keall, and R. Mohan, "Multileaf collimator transmission and scatter data for commissioning for dynamic intensity modulated radiotherapy," *Med. Phys.* (2000) (accepted).

¹³ Z. Chen, X. Wang, T. Bortfeld, R. Mohan, and L. E. Reinstein, "The influence of scatter on the design of the optimized intensity modulators," *Med. Phys.* **22**, 1727–1733 (1995).

¹⁴ R. Mohan, Q. Wu, X.-h. Wang, and J. Stein, "Intensity modulation optimization, lateral transport of radiation and margins," *Med. Phys.* **23**, 2011–2022 (1996).

¹⁵ J. V. Siebers, P. J. Keall, M. Arnfield, J. O. Kim, and R. Mohan, "Modeling of MLCs for MC-IMRT," Proceedings of the XIII International Conference on the Use of Computers in Radiation Therapy, Heidelberg, Germany, 2000 (accepted).

¹⁶ B. H. Press, A. Teukolsky, W. T. Vetterling, and B. P. Flannery, *Numerical Recipes in C: The Art of Scientific Computing* (Cambridge University Press, New York, 1992).